Controling the coupling properties of active ultrahigh-Q WGM microcavities from undercoupling to selective amplification

Alphonse Rasoloniaina, Vincent Huet, Thi Kim Ngan Nguyen, Elodie Le Cren, Michel Mortier, Laurent Michely, Yannick Dumeige, Patrice Féron

Correspondence and
requests for materials
should be addressed to
Y.D. (yannick.
dumeige@univ-
rennes1.fr)

Controling the coupling properties of active ultrahigh-Q WGM microcavities from undercoupling to selective amplification

A. Rasoloniaina[1], V. Huet[1], T. K. N. Nguyên[1], E. Le Cren[1], M. Mortier[2], L. Michely[2], Y. Dumeige[1] & P. Féron[1]

[1]FOTON (CNRS-UMR 6082), Université de Rennes I, ENSSAT, 6 rue de Kerampont, CS 80518, 22305 Lannion cedex, France, [2]LCMCP (CNRS-UMR 7574), Chimie-Paristech, 11 rue Pierre et Marie Curie, 75005 Paris, France.

Ultrahigh-quality (Q) factor microresonators have a lot of applications in the photonics domain ranging from low-threshold nonlinear optics to integrated optical sensors. Glass-based whispering gallery mode (WGM) microresonators are easy to produce by melting techniques, however they suffer from surface contamination which limits their long-term quality factor to a few 10^8. Here we show that an optical gain provided by erbium ions can compensate for residual losses. Moreover it is possible to control the coupling regime of an ultrahigh Q-factor three port microresonator from undercoupling to spectral selective amplification by changing the pumping rate. The optical characterization method is based on frequency-swept cavity-ring-down-spectroscopy. This method allows the transmission and dispersive properties of perfectly transparent microresonators and intrinsic finesses up to 4.0×10^7 to be measured. Finally we characterize a critically coupled fluoride glass WGM microresonator with a diameter of 220 μm and a loaded Q-factor of 5.3×10^9 is demonstrated.

D ue to their spectral selectivity and long photon lifetimes, very high-quality (Q) factor whispering-gallery-mode[1] (WGM) resonators have attractive functionalities for integrated or miniaturized photonics. In particular, it has been demonstrated that they can find applications in very sensitive sensing[2,3], microwave signal generation[4,5] or optical processing[6–11], narrow-band and high-contrast optical filtering[12,13] or high-coherence optical sources[14–18]. Although huge technological progresses have been done in chip-compatible integrated optics[19], crystalline millimeter size WGM resonators obtained by thorough cleaning and polishing steps provide the highest resonance quality[20,21] with Q-factors up to 10^{11}. Another approach to reach very high Q-factors consists in using WGM resonators made of materials with optical gain[22–25]. The internal amplification is used to compensate for optical losses coming from surface absorption due for example to chemosorbed OH$^-$ ions in silica WGM resonators[26–28] or surface scattering[29]. Moreover the pumping rate of the active medium give an additional degree of freedom to control the properties of the resonator[30,31]. In this paper, we present a new experimental configuration with a three port WGM rare-earth-doped microsphere: a dual in and out signal port and a third port which is used to inject the pump inside the WGM microsphere. This convenient experimental setup permits us to explore all the coupling regimes from undercoupling to spectral selective amplification in fluoride glass erbium-doped WGM microspheres. The coupling regime is infered from a careful analysis of the ringdown signal recorded using a frequency swept input signal[30]. In particular we show that this experimental technique can be used to obtain the dispersive properties of a highly transparent microsphere equivalent to a Gires-Tournois interferometer. Furthermore the technique is applied to measure very high intrinsic finesse values up to 4.0×10^7 associated with very low single pass absorption or ultrahigh Q-factors ($>5 \times 10^9$) without the use of a fine-stabilized Laser[21].

Results

System description. Figure 1 is a sketch of the experimental configuration. The evanescent tail of the mode of a tapered fiber is side coupled to the active WGM microcavity with the amplitude $u(t)$. The coupling photon lifetime is denoted τ_e. The intrinsic cavity photon lifetime τ_0 can be tailored by tuning the pumping rate through a half tapered fiber used to inject the pump field within the WGM microcavity. We assume that all the pumping
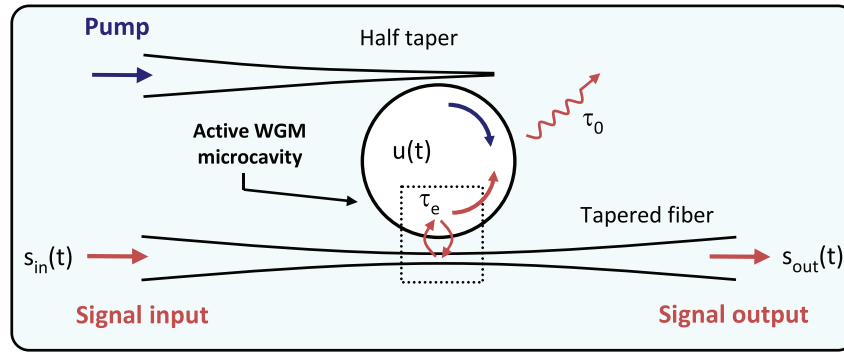
Figure 1 | Schematic view of a three-port WGM erbium-doped microsphere. The signal is coupled thanks to a tapered fiber and the pump beam is coupled through the half taper.

effects (including the losses due to the pump taper signal scattering) are taken into account by the value of τ_0[30]: $\tau_0 \geq 0$ for a passive cavity, in the case of an amplifying cavity $-\tau_e < \tau_0 < 0$. In the high-finesse cavity assumption (all the resonators experimentally studied in this paper have a finesse $F > 2.5 \times 10^6$), the output signal amplitude $s_{out}(t)$ is deduced from the input signal amplitude $s_{in}(t)$ by solving the following differential equation[32,34]:

$$\begin{cases} \dfrac{du}{dt} = \left(j\omega_0 - \dfrac{1}{\tau} \right) u(t) + \sqrt{\dfrac{2}{\tau_e}} s_{in}(t) \\ s_{out}(t) = -s_{in}(t) + \sqrt{\dfrac{2}{\tau_e}} u(t), \end{cases} \quad (1)$$

where ω_0 is the cavity resonance angular frequency. The amplitude cavity lifetime τ is defined by $1/\tau = 1/\tau_0 + 1/\tau_e$ and is related to the quality factor $Q = \omega_0/\Delta\omega$ of the cavity by $Q = \omega_0\tau/2$, here $\Delta\omega = 2/\tau$ is the cavity linewidth (in angular frequency units). In the linear stationary regime, the input signal can be written: $s_{in}(t) = \mathcal{S}_{in} \exp(j\omega t)$, and the system is fully described by its amplitude transfer function $h = s_{out}/s_{in}$:

$$h(\omega) = \sqrt{T(\omega)} \exp[j\phi(\omega)] = \frac{1/\tau_e - 1/\tau_0 - j(\omega - \omega_0)}{1/\tau_e + 1/\tau_0 + j(\omega - \omega_0)}. \quad (2)$$

The power transmission $T(\omega) = |h(\omega)|^2$ measured through the output port is given by:

$$T(\omega) = \frac{(1/\tau_e - 1/\tau_0)^2 + (\omega - \omega_0)^2}{(1/\tau_e + 1/\tau_0)^2 + (\omega - \omega_0)^2}. \quad (3)$$

For a detuned cavity ($|\omega - \omega_0| \to \pm\infty$) we have $T(\omega) \to 1$ which comes from the fact that for a high-finesse (passive) resonator the antiresonance transmission values are such as $T_{ar} = 1 + \mathcal{O}\left(\frac{1}{F^2}\right)$. At resonance ($\omega = \omega_0$) we can observe a dip with a Lorentzian shape ($T(\omega_0) \leq 1$) in the case of a passive cavity or a Lorentzian peak ($T(\omega_0) > 1$) for an amplifying microresonator. The dispersion properties can be characterized by the group delay experienced by the system, it can be extracted from the induced phase shift on the input signal obtained from the phase shift $\phi(\omega)$ by $\tau_g(\omega) = -\dfrac{d\phi}{d\omega}$. In particular the resonant group delay is given by[33]:

$$\tau_g(\omega_0) = \frac{2\tau_e\tau_0^2}{\tau_0^2 - \tau_e^2}. \quad (4)$$

The absolute and relative values of τ_0 and τ_e determine the coupling regime of the system:

- $0 < \tau_0 < \tau_e$ *undercoupling*: $0 < T(\omega_0) < 1$ and $\tau_g(\omega_0) < 0$
- $\tau_0 = \tau_e$ *critical coupling*[34]: $T(\omega_0) = 0$ and $\tau_g(\omega_0) \to \pm\infty$

- $\tau_e < \tau_0$ *overcoupling*: $0 < T(\omega_0) < 1$ and $\tau_g(\omega_0) > 0$
- $\tau_0 \to +\infty$ *transparent cavity*: $T(\omega_0) = 1$ and $\tau_g(\omega_0) = 2\tau_e$
- $\tau_0 < -\tau_e$ *frequency selective amplification*[35]: $T(\omega_0) > 1$ and $\tau_g(\omega_0) > 0$.

$\tau_g > 0$ corresponds to a slow-light regime whereas $\tau_g < 0$ is associated with a fast-light regime[36–39]. Ultrahigh-Q factor microcavities can have various applications depending on the operating regime. In the critical coupling, due to their wide free spectral range, microresonators can be used as selective notch filters. Used in the overcoupling, transparent or selective amplification regimes a microresonator behaves like an integrated delay line. In particular, the system can be a pure phase-shifter when the cavity is at transparency. An efficient resonant net gain can be obtained in the case of the selective amplification regime. From a practical point of view a thorough optical characterization is required to determine the properties of high-Q microresonators. The method usually carried out consists in using a very narrow-linewidth Laser which carrier angular frequency is linearly swept in time as input signal[34,40]: $\omega(t) = \omega_i + V_S t/2$. The bandwidth of the power transmission function $T(\omega)$ is deduced from the trace of the transmission $T(t)$ in the time domain. To insure a stationary regime, the frequency sweeping rate V_S has to be very slow compared to the sweeping speed $V_0 = 4/\tau^2$ corresponding to one resonance scanned during the cavity lifetime. In Figure 2(a), the transmission $T(t)$ of a critically coupled cavity and a very slow sweeping speed ($V_S = 10^{-3} V_0$) is displayed. The width of the resonance in the time domain is 500τ or $500\tau \times 10^{-3} V_0 = 2/\tau$ in the angular frequency domain. If the frequency speed is of the same order of magnitude as V_0, the dynamic of the cavity mode must be taken into account[21,30,41–43]. The amplitude of the field is given by:

$$u(t) = \sqrt{\frac{2}{\tau_e}} \mathcal{S}_{in} \exp(j\omega_0 t - t/\tau) \left[f(t) - f(0) + \frac{\tau}{1 + j(\omega_i - \omega_0)\tau} \right], \quad (5)$$

where we define:

$$f(t) = -\sqrt{\frac{j\pi}{2V_S}} \exp\left[-\frac{j(\omega_i - \omega_0 - j/\tau)^2}{2V_S} \right] \text{erf}\left(\frac{j/\tau + \omega_0 - \omega_i - V_S t}{\sqrt{2jV_S}} \right), \quad (6)$$

with erf(z) and $z \in \mathbb{C}$ denoting the complex error function. Using Eqs. (1), (5) and (6), we can obtain an analytical expression for $T(t)$. The transmission of the critically coupled cavity for a high speed frequency sweeping is plotted in Figure 2(c). The interference between the intracavity field and the input field creates some ringing oscillations on the transmission curve[41]. By analyzing this beat we determine the value of V_S which is difficult to calibrate precisely from an experimental point of view. In a similar manner, the ringing signal from the cavity, is used to infer the coupling regime for a passive resonator[30]. Note that in the stationary regime this can be done unambiguously solely by interferometric[44–46] or polarimetric[47–49] techniques. For a perfectly transparent cavity (lossless cavity $\tau_0 \to$
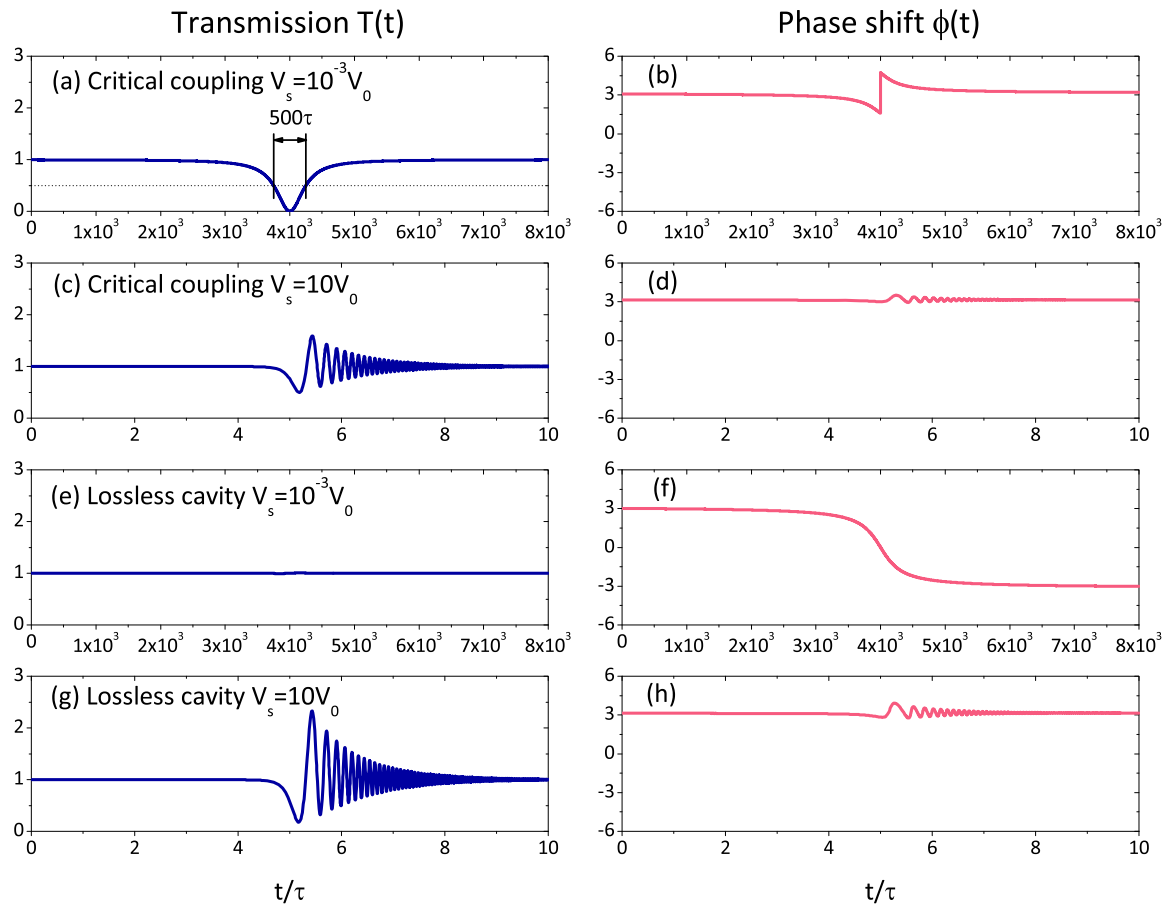
Figure 2 | Theoretical calculation of the transmission $T(t)$ and the phase shift $\phi(t)$ of the amplitude transfer function in the dynamic regime: (a)–(d) for a critically coupled resonator and (e)–(h) for a transparent (or lossless) cavity. We have used two different sweeping rates: (a), (b), (e) and (f) $V_S = 10^{-3}V_0$ almost corresponding to the stationary regime; (c), (d), (g) and (h) $V_S = 10V_0$.

$+\infty$), the power transmission is $T(\omega) = 1$ as can be seen in Fig. 2(e). Consequently in the stationary regime, information about the quality of the resonance and the dispersive properties of the cavity can only be obtained by measuring the phase shift $\phi(\omega) = 2 \arctan[(\omega_0 - \omega)\tau_e]$ [see Fig. 2(f)] using phase-sensitive methods[44]. When the frequency sweeping is high compared to V_0 [Fig. 2(g)], the properties of the resonator can be deduced from a thorough analysis of the induced ringing oscillations in the transmission profile. For $V_S \gtrsim 2V_0$, the resonator is not perfectly loaded and the 2π phase shift disappears as illustrated in Fig. 2(h).

Experimental setup. We used the experimental setup described in Fig. 3 to characterize the linear properties of erbium-doped ZBLALiP glass microspheres[50]. The fabrication process of the microspheres is described at section Methods. A counter-propagative pump field from a Laser diode at $\lambda_P = 1480$ nm is coupled to the resonator via a half-tapered fiber. Before starting the frequency sweeping of the probe signal, we identify and choose a resonance of the microcavity by analyzing its intrinsic emission with an optical spectrum analyzer (OSA). The probe signal reflected from the coupler C to the OSA is used to tune the probe Laser frequency to the chosen microsphere resonance. A narrow band tunable Laser operating around $\lambda_S = 1560$ nm is used as the frequency linearly scanned probe signal. The sweeping speed is around $V_S \approx 2\pi \times 1$ MHz/μs which approximately corresponds to $4V_0$ for a quality factor $Q = 10^9$. The input probe signal is coupled to the WGM resonator via a tapered fiber. The coupling conditions (τ_e) can be adjusted by varying the distance between the microsphere and the taper. The mode matching between the pump and the probe waves is

optimized by selecting the pump wavelength in the vicinity of the probe, here 1480 nm and 1560 nm. The signal extracted from the microsphere is first optically amplified by an erbium-doped fiber amplifier and then filtered with a narrow bandpass tunable filter (see section Methods). An amplified fast photodiode collects the output optical signal.

Measurements. In Fig. 4 and Fig. 5 the ringing profiles $T(t)$ obtained for two erbium-doped microspheres with two different concentrations and diameters D are shown. In these experiments we applied a pump power P_P (defined in Fig. 3) between 3 mW and 11.4 mW. The power of the probe signal P_S was chosen between 115 nW and 550 nW in order to avoid gain saturation. The ringing profiles are fitted using the analytical expressions given previously and the procedure described at the section Methods. As explained before, from the fit of the curves, we deduce τ_0, τ_e as well as a (relatively) precise calibration of the frequency sweeping rate V_S. The values of the two cavity lifetimes τ_0 and τ_e fully characterize the linear properties of the microresonator, they give the coupling regime, the intrinsic Q-factor $Q_0 = \omega_0\tau_0/2$, the loaded Q-factor Q, the resonant transmission (or gain) and the resonant group delay. All the experimental data have been gathered in Tab. I and plotted in the graph at Fig. 6 which shows the resonant transmission and group delay as a function of the intrinsic photon lifetime.

Discussion

With the various microspheres all the different coupling regimes have been reached. For example, plot D of Fig. 5 shows a nearly perfect case of a critically coupled resonator. In the stationary regime
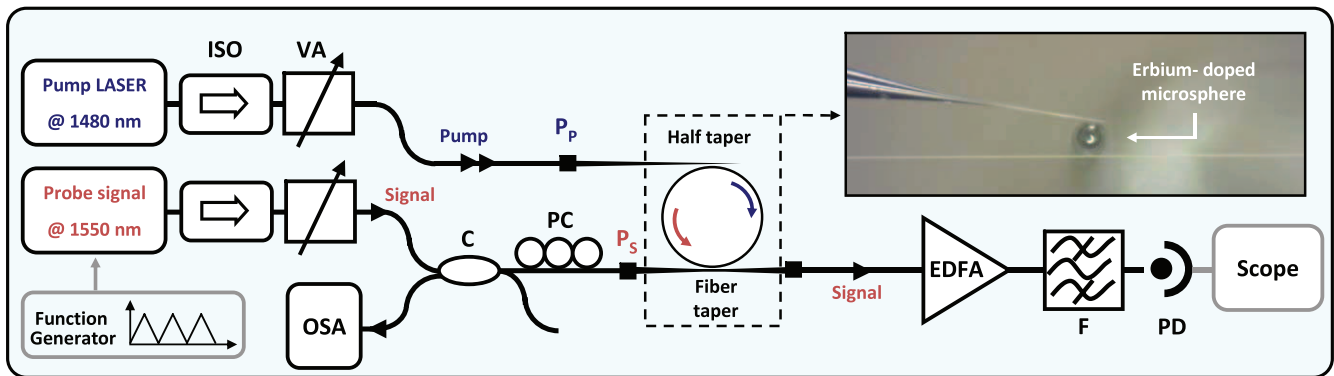
Figure 3 | Experimental setup. ISO: optical isolator, VA: variable attenuator, OSA: optical spectrum analyzer, C: 3 dB coupler, PC: polarization controller, EDFA: Erbium-doped fiber amplifier, F: optical filter, PD: Amplified photodiode. P_P and P_S are respectively the pump and signal power at the taper inputs.

such a resonator used as a notch filter would give a rejection of about 52 dB. From the fit of plot H (Fig. 4) we deduce an intrinsic Q-factor $Q_0 = 1.1 \times 10^{10}$, for this resonator this corresponds to a loss-limited finesse $F_0 = \lambda_0 Q_0/(n\pi D) \approx 4.0 \times 10^7$ or a single-pass intensity absorption $1 - a^2 = 2\pi/F_0 = 1.6 \times 10^{-7}$ assuming a refractive index $n = 1.5$ and $\lambda_0 = 2\pi c/\omega_0 = 1560$ nm. In the case of a nearly transparent cavity as shown in plot I (Fig. 4) where $Q_0 \gg Q$, the stationary transmission spectrum would be $T(\omega) = 1$ as theoretically shown in Fig. 2(e), unfortunately the phase shift properties of the resonator could not be measured. Using the transient analysis we can extract the coupling rate ($\tau_e = 1.5$ μs) and deduce the dispersive properties of the system. Plot K (Fig. 5) is an example of a strongly resonant amplifier with a maximal gain of 19 dB associated with a bandwidth of 180 kHz. Finally, for a 220 μm diameter 0.1 mol.% erbium-doped microsphere we give in Fig. 7 a ringing profile corresponding to a loaded quality factor $Q = 5.3 \times 10^9$ next to the critical coupling.

As a conclusion, we show here that the internal gain provided by the active medium of the cavity can be a way to compensate for glass-material limitation and permits the achievement of very high-Q optical microresonators up to 5×10^9. Depending on the coupling regime, erbium-doped microspheres can carry out diverse functions. i) At critical coupling, they can be used as a very selective notch filters with high rejection ratio. The frequency bandwidth of such a filter is $2/(\pi\tau_0)$. For a passive microresonator, it is thus limited by optical losses and set for a given structure whereas in the case of an active system, the bandwidth can be adjusted by tuning the pumping rate of the resonator. ii) Loss-compensated ($Q_0 \rightarrow +\infty$) cavities could be used as transparent delay lines with a maximal delay $\tau_g(\omega_0) = 2\tau_e$ that can be changed by modifying the coupling rate between the resonator and the access line. We have also shown that the cavity-ring-down-spectroscopy applied to loss-compensated resonators permits to measure their linear properties which is not possible when simply measuring the stationary power transmission $T(\omega)$. Moreover, very small absorption or ultrahigh intrinsic Q-factor Q_0 can be measured with this method which implies possible applications in the domain of very sensitive sensors. iii) Finally in the spectral
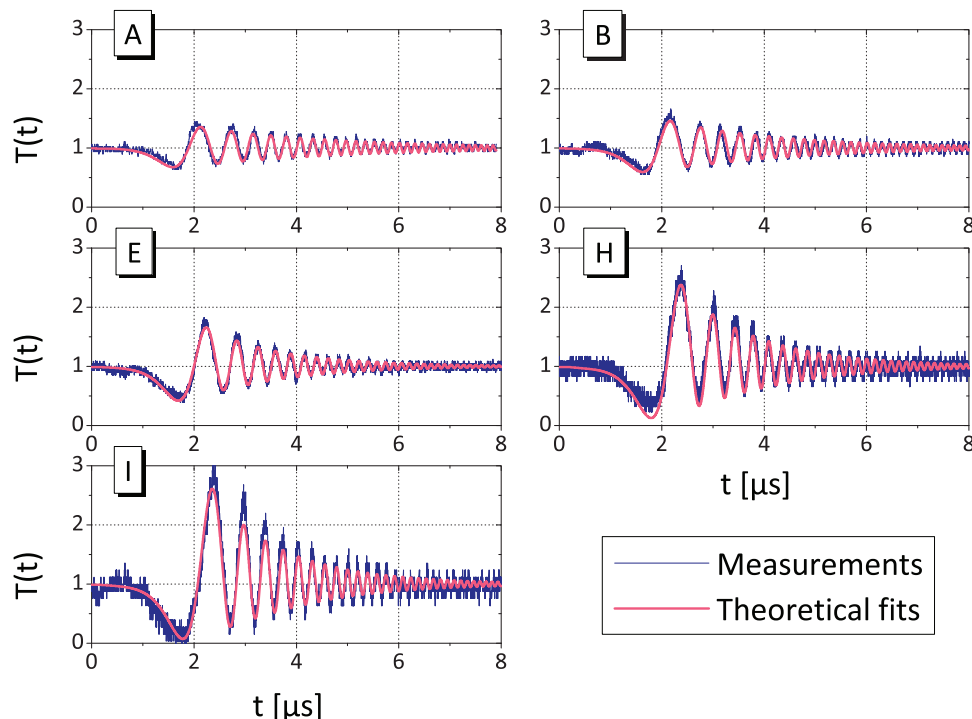

Figure 4 | Ringing profile recorded for two ZBLALiP microspheres for a 0.08 mol.% erbium-doped, $D = 90$ μm diameter microsphere. The resonant transmissions $T(\omega_0)$ and resonant group delays $\tau_g(\omega_0)$ deduced from the fits of the experimental curves A, B, E, H and I are reported in Fig. 6.
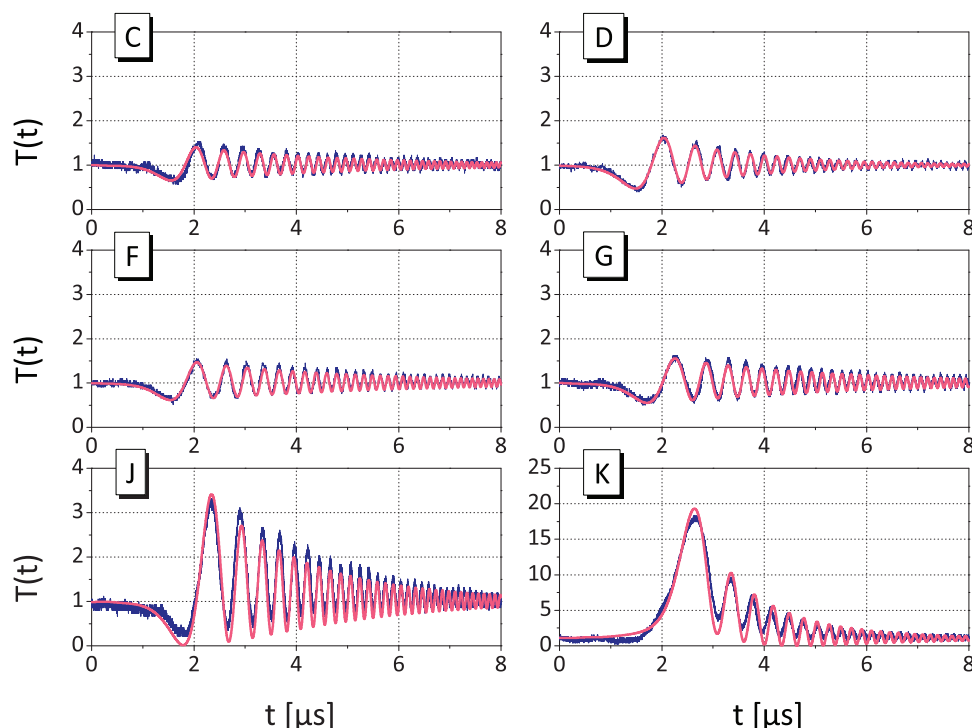
Figure 5 | Ringing profile recorded for two ZBLALiP microspheres for a 0.1 mol.% erbium-doped, D = 145 μm diameter microsphere. The resonant transmissions $T(\omega_0)$ and resonant group delays $\tau_g(\omega_0)$ deduced from the fits of the experimental curves C, D, F, G, J and K are reported in Fig. 6.

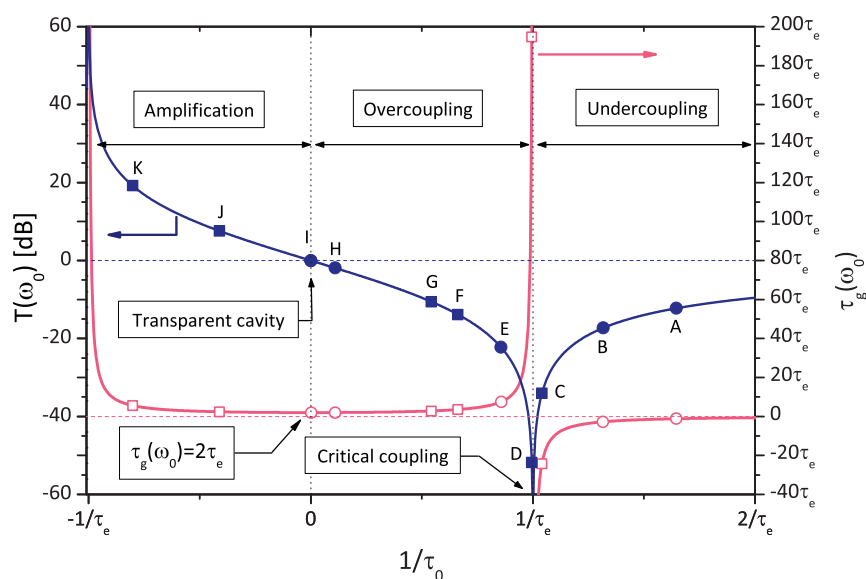| Table I	Inferred linear parameters obtained from fitting of ringing profiles given in Fig. 4 and Fig. 5					
	τ_0	τ_e	Q_0	Q	$\tau_g(\omega_0)$	$T(\omega_0)$
A	4.6 μs	7.6 μs	2.8×10^9	1.7×10^9	−9.0 μs	−12 dB
B	4.4 μs	5.7 μs	2.6×10^9	1.5×10^9	−16 μs	−17 dB
C	6.3 μs	6.6 μs	3.8×10^9	2.0×10^9	−160 μs	−34 dB
D	4.12 μs	4.10 μs	2.5×10^9	1.2×10^9	800 μs	−52 dB
E	3.7 μs	3.2 μs	2.2×10^9	1.0×10^9	24 μs	−22 dB
F	9.5 μs	6.3 μs	5.7×10^9	2.3×10^9	22 μs	−14 dB
G	10 μs	5.5 μs	6.1×10^9	2.1×10^9	16 μs	−11 dB
H	18 μs	1.9 μs	1.1×10^{10}	1.1×10^9	3.9 μs	−1.9 dB
I	$\tau_0 \gg \tau_e$	1.5 μs	$Q_0 \gg Q$	9.3×10^8	3.1 μs	≈0 dB
J	−3.3 μs	1.4 μs	/	1.4×10^9	3.3 μs	7.6 dB
K	−0.44 μs	0.35 μs	/	1.1×10^9	2.0 μs	19 dB

Figure 6 | Resonant transmission and group delay obtained from the fitting of the ringing profiles A-K provided in Fig. 4 and Fig. 5.
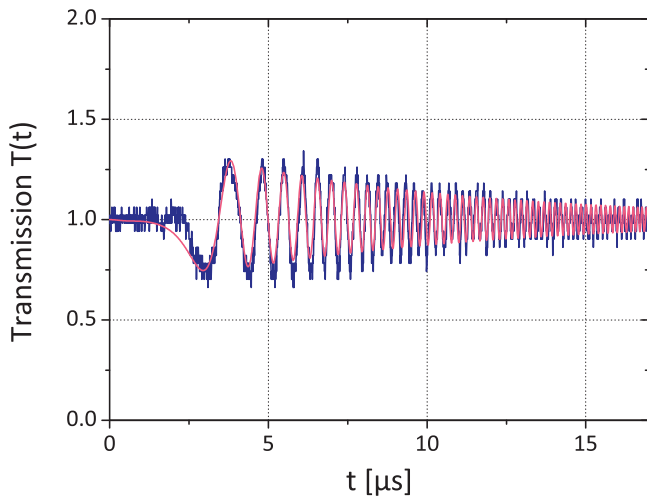
Figure 7 | Ringing profile measured from a 0.1 mol.% erbium-doped microsphere D = 220 μm diameter microsphere. $\tau_0 = 17.3$ μs, $\tau_e = 17.5$ μs and thus $Q = 5.3 \times 10^9$.

selective amplification regime, erbium-doped WGM resonator could be used as narrow-band amplifying filter for microwave or high-coherence photonic applications[8,10].

Methods

Microsphere fabrication. The process is based on a microwave plasma torch which enables us to produce microspheres by melting of ZBLALiP glass[50] powders. The plasma is generated using a microwave supply with a nominal oscillator frequency of 2.4 GHz and a power of 160 W. Argon (3 L/min output) is used as plasma gas and oxygen (4 L/min output) as sheath gas. Powders are axially injected and melt when passing through the plasma flame. Surface tension generates their spherical shape. Free spheres are collected down the chamber. The diameter of the spheres depends essentially on the grain size and varies from 10 to 250 μm. The spheres are then glued at the tip of drawn optical fibers (20 μm) permitting an easy handling.

Description of the experimental setup. The two tapers have a diameter smaller than 2 μm. The position of the microsphere is set and the two tapers are mounted on 3-axis micro-positioning stages in order to control their relative distance (typically less than the wavelength). The probe Laser is an external cavity Laser diode in the C-band ($\lambda_S \approx$ 1560 nm) with a long-term linewidth of 150 kHz. The Laser frequency is linearly swept over 6 GHz using a 100 Hz triangle 18 V peak to peak signal. The input signal power P_S (Fig. 3) is weak (a few hundred nW) in order to avoid gain saturation inside the microsphere. Moreover due to taper aging during the experiments, insertion losses are such as we have to use an EDFA as optical preamplifier. The EDFA is a low noise amplifier with a maximal output of 18 dBm. An optical filter (F) is used to reject the amplified spontaneous emission (both from the EDFA and the microsphere) and the scattered pump signal. It is tunable in the range 1450–1650 nm and it has a minimal bandwidth around 6.25 GHz. The photodiode has a bandwidth of 1.2 GHz with a transimpedance gain between 10^2 and 10^4 V/A and a rise time between 1.8 and 25 ns. The pump Laser is a multimode Laser diode emitting at $\lambda_P \approx$ 1480 nm with a maximal power of 150 mW.

Cavity lifetime measurement procedure. The experimental transmission signal $T_{exp}(t)$ is normalized using the off-resonance value. In all our experiments $Q \gtrsim 10^9$ and thus the bandwidth of the resonator is lower than 200 kHz corresponding to 0.2 μs for a sweeping speed of $2\pi \times 1$ MHz/μs. From Fig. 4, Fig. 5 and Fig. 7 we can deduce that the off-resonance value is taken for a detuning corresponding to almost 10 times the resonator bandwidth. This leads to a relative error (compared to the maximal transmission) less than 1% even for strongly amplifying resonators. The experimental signal is then compared to the theoretical signal $T_{theo}(t)$ depending on τ_0, τ_e and V_S calculated from Eqs. (5) and (6). A nonlinear optimization procedure on τ_0, τ_e and V_S is used to minimize the value of σ^2 which reads:

$$\sigma^2(\tau_0, \tau_e, V_S) = \sum_{k=1}^{N} \left[T_{exp}(t_k) - T_{theo}(t_k, \tau_0, \tau_e, V_S) \right]^2, \quad (7)$$

where N is the number of experimental sampling points. In the general case we have checked that the error on the measurements was less than 10%. For critical coupling (plot D), where the relative value of τ_0 and τ_e is crucial for the determination of $T(\omega_0)$, we carried out several runs of optimization with very different starting points. All the inferred data were different by less than 0.1%. The method has been validated using fiber resonators[30] for which the coupling coefficients can be independently measured. For a long four-port fiber resonator[51]

(length of 20 m and two 99%/1% couplers), we have checked the consistency of the method for overall Q-factors up to 3.3×10^9.

1. Chiasera, A. *et al.* Spherical whispering-gallery-mode microresonators. *Laser Photon. Rev.* **4**, 457–482 (2010).
2. Vollmer, F. *et al.* Protein detection by optical shift of a resonant microcavity. *Appl. Phys. Lett.* **80**, 4057–4059 (2002).
3. Ward, J. & Benson, O. WGM microresonators: sensing, lasing and fundamental optics with microspheres. *Laser Photon. Rev.* **5**, 553–570 (2011).
4. Savchenkov, A. A. *et al.* Low threshold optical oscillations in a whispering gallery mode CaF$_2$ resonator. *Phys. Rev. Lett.* **93**, 243905 (2004).
5. Xiao, L. *et al.* Miniaturized optical microwave source using a dual-wavelength whispering gallery mode laser. *IEEE Photon. Technol. Lett.* **22**, 559–561 (2010).
6. Ilchenko, V. S., Savchenkov, A. A., Matsko, A. B. & Maleki, L. Whispering-gallery-mode electro-optic modulator and photonic microwave receiver. *J. Opt. Soc. Am. B* **20**, 333–342 (2003).
7. Savchenkov, A. A. *et al.* Single-sideband electro-optical modulator and tunable microwave photonic receiver. *IEEE Trans. Microw. Theory Techn.* **58**, 3167–3174 (2010).
8. Volyanskiy, K. *et al.* Compact optoelectronic microwave oscillators using ultra-high Q whispering gallery mode disk-resonators and phase modulation. *Opt. Express* **18**, 22358–22363 (2010).
9. Savchenkov, A. A. *et al.* Voltage-controlled photonic oscillator. *Opt. Lett.* **35**, 1572–1574 (2010).
10. Merrer, P.-H. *et al.* Characterization technique of optical whispering gallery mode resonators in the microwave frequency domain for optoelectronic oscillators. *Appl. Phys. Lett.* **51**, 4742–4748 (2012).
11. Coillet, A. *et al.* Time-domain dynamics and stability analysis of optoelectronic oscillators based on whispering-gallery mode resonators. *IEEE J. Sel. Top. Quantum Electron.* **19**, 6000112 (2013).
12. Spillane, S. M., Kippenberg, T. J., Painter, O. J. & Vahala, K. J. Ideality in a fiber-taper-coupled microresonator system for application to cavity quantum electrodynamics. *Phys. Rev. Lett.* **91**, 043902 (2003).
13. Savchenkov, A. A. *et al.* Narrowband tunable photonic notch filter. *Opt. Lett.* **34**, 1318–1320 (2009).
14. Sandoghdar, V. *et al.* Very low threshold whispering-gallery-mode microsphere laser. *Phys. Rev. A* **54**, R1777–R1780 (1996).
15. Lissillour, F., Gabet, R., Féron, P., Besnard, P. & Stéphan, G. Linewidth narrowing of a DFB semiconductor laser at 1.55 μm by optical injection of an Er:ZBLAN microspherical laser. *Europhys. Lett.* **55**, 499–504 (2001).
16. Sprenger, B., Schwefel, H. G. L. & Wang, L. J. Whispering-gallery-mode-resonator-stabilized narrow-linewidth fiber loop laser. *Opt. Lett.* **34**, 3370–3372 (2009).
17. Liang, W. *et al.* Whispering-gallery-mode-resonator-based ultranarrow linewidth external-cavity semiconductor laser. *Opt. Lett.* **35**, 2822–2824 (2010).
18. Rivera-Pérez, E., Díez, A., Andrés, M. V., Cruz, J. L. & Rodríguez-Cobos, A. Tunable narrowband fiber laser with feedback based on whispering gallery mode resonances of a cylindrical microresonator. *Opt. Lett.* **38**, 1636–1638 (2013).
19. Lee, H. *et al.* Chemically etched ultrahigh-Q wedge-resonator on a silicon chip. *Nat. Photon.* **6**, 369–373 (2012).
20. Grudinin, I. S., Ilchenko, V. S. & Maleki, L. Ultrahigh optical Q factors of crystalline resonators in the linear regime. *Phys. Rev. A* **74**, 063806 (2006).
21. Savchenkov, A. A., Matsko, A. B., Ilchenko, V. S. & Maleki, L. Optical resonators with ten million finesse. *Opt. Express* **15**, 6768–6773 (2007).
22. Hsiao, H. & Winick, K. A. Planar glass waveguide ring resonators with gain. *Opt. Express* **15**, 17783–17797 (2007).
23. Totsuka, K. & Tomita, M. Optical microsphere amplification system. *Opt. Lett.* **32**, 3197–3199 (2007).
24. He, L., Ozdemir, S. K., Xiao, Y.-F. & Yang, L. Gain-Induced Evolution of Mode Splitting Spectra in a High-Q Active Microresonator. *IEEE J. Quantum Electron.* **46**, 1626–1633 (2010).
25. Rasoloniaina, A. *et al.* High-gain wavelength-selective amplification and cavity ring down spectroscopy in a fluoride glass erbium-doped microsphere. *Opt. Lett.* **37**, 4735–4737 (2012).
26. Gorodetsky, M. L., Savchenkov, A. A. & Ilchenko, V. S. Ultimate Q of optical microsphere resonators. *Opt. Lett.* **21**, 453–455 (1996).
27. Kippenberg, T. J., Tchebotareva, A. L., Kalkman, J., Polman, A. & Vahala, K. J. Purcell-factor-enhanced scattering from Si nanocrystals in an optical microcavity. *Phys. Rev. Lett.* **103**, 027406 (2009).
28. Trebaol, S., Dumeige, Y. & Féron, P. Ringing phenomenon in coupled cavities: Application to modal coupling in whispering-gallery-mode resonators. *Phys. Rev. A* **81**, 043828 (2010).
29. Vernooy, D. W., Ilchenko, V. S., Mabuchi, H., Streed, E. W. & Kimble, H. J. High-Q measurements of fused-silica microspheres in the near infrared. *Opt. Lett.* **23**, 247–249 (1998).
30. Dumeige, Y. *et al.* Determination of coupling regime of high-Q resonators and optical gain of highly selective amplifiers. *J. Opt. Soc. Am. B* **25**, 2073–2080 (2008).
31. Tomita, M., Ueta, T. & Sultana, P. Slow optical pulse propagation in an amplifying ring resonator. *J. Opt. Soc. Am. B* **28**, 1627–1630 (2011).
32. Haus, H. *Waves and fields in optoelectronics* (Prentice-Hall, 1984).

33. Cai, M., Painter, O. & Vahala, K. J. Observation of critical coupling in a fiber taper to a silica-microsphere whispering-gallery mode system. *Phys. Rev. Lett.* **10**, 74–77 (2000).

34. Trebaol, S. *et al.* Artificial dispersion of active optical coupled resonator systems. *C. R. Phys. (Paris)* **10**, 964–979 (2009).

35. Choi, J. M., Lee, R. K. & Yariv, A. Control of critical coupling in a ring resonator–fiber configuration: application to wavelength-selective switching, modulation, amplification, and oscillation. *Opt. Lett.* **26**, 1236–1238 (2001).

36. Heebner, J. E., Boyd, R. W. & Park, Q.-H. Slow light, induced dispersion, enhanced nonlinearity, and optical solitons in a resonator-array waveguide. *Phys. Rev. E* **65**, 036619 (2002).

37. Heebner, J. E., Wong, V., Schweinsberg, A., Boyd, R. W. & Jackson, D. J. Optical transmission characteristics of fiber ring resonators. *IEEE J. Quantum Electron.* **40**, 726–730 (2002).

38. Totsuka, K. & Tomita, M. Dynamics of fast and slow pulse propagation through a microsphere-optical-fiber system. *Phys. Rev. E* **75**, 016610 (2007).

39. Tomita, M., Uesugi, H., Sultana, P. & Oishi, T. Causal information velocity in fast and slow pulse propagation in an optical ring resonator. *Phys. Rev. A* **84**, 043843 (2011).

40. Armani, D. K., Kippenberg, T. J., Spillane, S. M. & Vahala, K. J. Ultra-high-Q toroid microcavity on a chip. *Nature* **421**, 925–928 (2003).

41. Ioannidis, Z. K., Radmore, P. M. & Giles, I. P. Dynamic response of an all-fiber ring resonator. *Opt. Lett.* **13**, 422–424 (1988).

42. Poirson, J., Bretenaker, F., Vallet, M. & Le Floch, A. Analytical and experimental study of ringing effects in a Fabry-Perot cavity. Application to the measurement of high finesses. *J. Opt. Soc. Am. B* **14**, 2811–2817 (1997).

43. Morville, J., Romanini, D., Chenevier, M. & Kachanov, A. Effects of laser phase noise on the injection of a high-finesse cavity. *Appl. Opt.* **41**, 6980–6990 (2002).

44. Slagmolen, B. J. J., Gray, M. B., Baigent, K. G. & McClelland, D. E. Phase-sensitive reflection technique for characterization of a Fabry-Perot interferometer. *Appl. Opt.* **39**, 3638–3643 (2000).

45. Michaud-Belleau, V. *et al.* Whispering gallery mode sensing with a dual frequency comb probe. *Opt. Express* **20**, 3066–3075 (2012).

46. Bergeron, H. *et al.* Optical impulse response of silica microspheres: Complementary approach to whispering-gallery-mode analysis. *Phys. Rev. A* **87**, 063835 (2013).

47. Tanaka, A. *et al.* Phase shift spectra of a fiber–microsphere system at the single photon level. *Opt. Express* **19**, 2278–2285 (2011).

48. Vanier, F., La Mela, C., Hayat, A. & Peter, Y.-A. Intrinsic quality factor determination in whispering gallery mode microcavities using a single Stokes parameters measurement. *Opt. Express* **19**, 23544–23553 (2011).

49. Fujiwara, M. *et al.* Coupling of ultrathin tapered fibers with high-Q microsphere resonators at cryogenic temperatures and observation of phase-shift transition from undercoupling to overcoupling. *Opt. Express* **20**, 19545–19553 (2012).

50. Mortier, M. *et al.* New fluoride glasses for laser applications. *J. Non-Cryst. Solids* **326 & 327**, 505–509 (2003).

51. Trebaol, S. Etudes expérimentales des propriétés dispersives de structures photoniques à base de micro-résonateurs pour la réalisation de fonctions optiques. *PhD thesis* (Université de Rennes 1, France, 2010).

Acknowledgments

Author contributions

A.R. and V.H. performed the experiments, A.R., V.H., N.T.K.N. and E.L.C. contributed to develop the experimental setup. M.M. and L.M. made all the glass samples. The design of the experiment and the signal analysis were developed by Y.D. and P.F. All authors reviewed the manuscript.

Additional information

ERRATUM: Controling the coupling properties of active ultrahigh-Q WGM microcavities from undercoupling to selective amplification

A. Rasoloniaina, V. Huet, T. K. N. Nguyên, E. Le Cren, M. Mortier, L. Michely, Y. Dumeige & P. Féron

This Article contains errors in the numbering of two papers in the reference list. Reference 33 and 34 are incorrectly listed as 34 and 33, respectively. The correct numbering appears below:

33. Trebaol, S. *et al.* Artificial dispersion of active optical coupled resonator systems. *C. R. Phys. (Paris)* **10**, 964–979 (2009).

34. Cai, M., Painter, O. & Vahala, K. J. Observation of critical coupling in a fiber taper to a silica-microsphere whispering-gallery mode system. *Phys. Rev. Lett.* **10**, 74–77 (2000).